

See discussions, stats, and author profiles for this publication at: <https://www.researchgate.net/publication/281784272>

Ultrafast Microwave Welding/Reinforcing Approach at the Interface of Thermoplastic Materials

ARTICLE in ACS APPLIED MATERIALS & INTERFACES · SEPTEMBER 2015

Impact Factor: 6.72 · DOI: 10.1021/acsmami.5b06484

READS

20

4 AUTHORS, INCLUDING:



[Selcuk Poyraz](#)

Namık Kemal Üniversitesi

16 PUBLICATIONS 192 CITATIONS

[SEE PROFILE](#)



[Lin Zhang](#)

Auburn University

23 PUBLICATIONS 258 CITATIONS

[SEE PROFILE](#)



[Xinyu Zhang](#)

Auburn University

47 PUBLICATIONS 1,782 CITATIONS

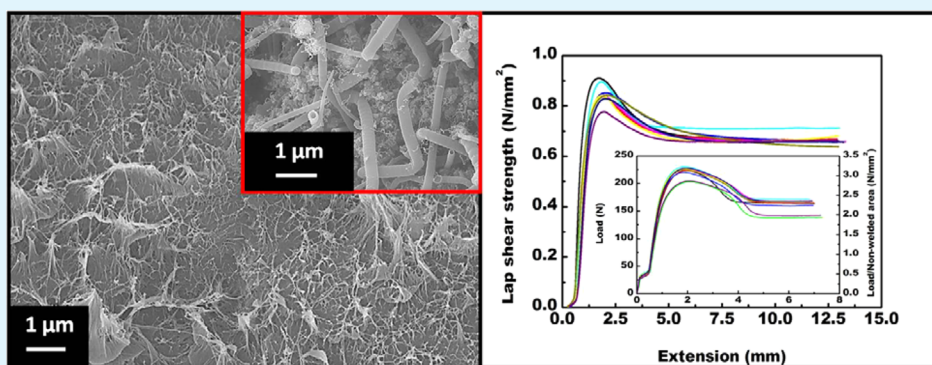
[SEE PROFILE](#)

Ultrafast Microwave Welding/Reinforcing Approach at the Interface of Thermoplastic Materials

Selcuk Poyraz,^{†,‡} Lin Zhang,[§] Albrecht Schroder,[†] and Xinyu Zhang^{*,†}

[†]Department of Chemical Engineering and [§]Materials Research and Education Center, Auburn University, Auburn, Alabama 36849, United States

[‡]Department of Textile Engineering, Corlu Faculty of Engineering, Namik Kemal University, Corlu, Tekirdag 59860, Turkey



ABSTRACT: As an attempt to address the needs and tackle the challenges in welding of thermoplastic materials (TPMs), a novel process was performed via short-term microwave (MW) heating of a specific composite, made up of conducting polypyrrole nanogranule (PPy NG) coated carbon and catalyst source precursor (ferrocene) fine particles, at substrate polypropylene (PP) dog bone pieces' interface. Upon vigorous interactions between MWs and electromagnetic absorbent PPy NG coating, the energy was transformed into a large amount of heat leading to a drastic temperature increase that was simultaneously used for the instant carbonization of PPy and the decomposition of fine ferrocene particles, which resulted in multiwalled carbon nanotubes (CNTs) growth at the interface. Meanwhile, the as-grown CNTs on the surface conveyed the heat into the adjacent bulk PP and caused locally molten surface layers' formation. Eventually, the light pressure applied at the interface during the heating process squeezed the molten layers together and a new weld was generated. The method is considerably advantageous compared to other alternatives due to (i) its fast, straightforward, and affordable nature, (ii) its applicability at ambient conditions without the need of any extra equipment or chemicals, and also (iii) its ability to provide clean, durable, and functional welds, via precisely controlling process parameters, without causing any thermal distortion or physical alterations in the bulk TPM. Thus, it is believed that this novel welding process will become much preferable for the manufacturing of next-generation TPM composites in large scale, through short-term MW heating.

KEYWORDS: *thermoplastic material, conducting polymer, microwave energy, welding, reinforcing*

INTRODUCTION

After their discovery in the early 20th century, thermoplastic materials' (TPMs) use became widespread following World War II, and since then, they had been utilized to reshape humans' daily lives from all aspects, and to replace numerous traditional materials like glass, wood, metal, or ceramic¹ in their field of applications as the new-generation structural materials.² The fairly elastic structure and chemically inert nature of TPMs, which originate from their long polymeric chains comprised of simple repetitive units,³ are the primary benefits of these materials. Besides that, TPMs' desirable⁴ physical (lightweight and lower density), mechanical (high specific strength, stiffness, and flexibility), thermal (lower processing temperatures), electrical (inert and insulating nature), and economical (affordable in bulk quantities) properties had been verily facilitating their uses.³ These materials' suitability for a wide

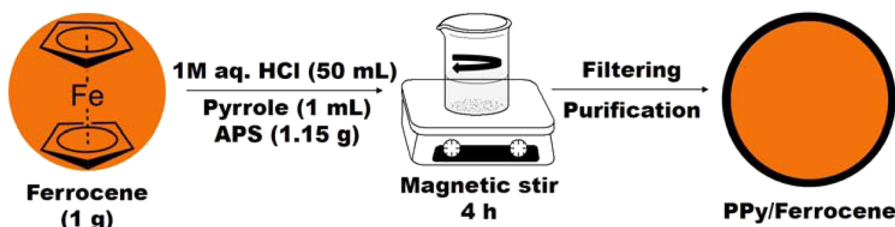
variety of manufacturing techniques, ease of processing via simple molding applications at relatively lower temperatures (compared to metals and their alloys), advantageous applicability into the automated mass production systems, and more importantly, their promising potential for the manufacturing of highly complex and multifunctional composite products that warrant strict requirements, enable them to become the materials of preference with much lower costs³ for a large span of structural and commercial applications in automotive,⁵ aerospace, and aeronautics industries.⁶ Moreover, the above-mentioned high-performance composites made up of TPMs have become a more viable alternative by providing decisive

Received: July 20, 2015

Accepted: September 15, 2015



Scheme 1. Illustration of the One-Step PPy/Ferrocene Composite Synthesis



advantages of being more cost-effective⁵ and facilely reprocesable and having greater damage tolerance than the thermoset resin-based ones.²

As an attempt to address the needs in processing (joining and/or repairing damaged interfaces)^{3,7–9} of TPMs in a quicker and more efficient manner, various types of welding approaches have been developed such as resistive implantation,¹⁰ heat conduction,³ induction heating,³ ultrasonic welding,¹⁰ flash welding,¹¹ laser welding,^{12,13} and microwave (MW) welding.^{4,10,12–15} Primarily, joining of parts was done either by adhesive bonding or by mechanical fastening,^{2,3} but after the development of such welding applications, more effective processes have become accessible and easily applicable to TPMs. Eventually, in some cases, mechanically more robust, residual stress concentrated point-free and impurity/dislocation-free joints with mechanical properties as high as the bulk material could be obtained.^{3,15,16}

Although it was primarily developed for communication purposes,^{7,9,14} and had been extensively¹⁷ used for various areas including cooking foodstuff,^{7,8} heating/thawing/drying of materials,^{5,9,14,18} curing thermoset materials, plasma generation for rubber vulcanization and processing of ceramics,^{1,2,7–9,12,14} the application of MW technology for the processing of materials, i.e., welding applications, was relatively a newer development⁸ that took place later on in 1960s.¹⁴ In contrast to the above-mentioned welding approaches' limitations, such as being complicated, time-consuming,¹⁹ and wasteful on bulk material, MW welding has a number of significant advantages. First of all, its working principle is based on volumetric heating of the material (all the way through at the same time)¹⁴ by electromagnetic irradiation at a certain frequency range^{5,9,12,14} (commonly 2.45 GHz) in the spectrum.^{2,5,19–21} This feature allows shorter process times, less power consumption, and higher efficiency in different materials' processing.^{7–9,14} Additionally, when this technology is particularly used for the welding of complex components, substantial savings can be made both in the initial investment cost of the equipment and during further processing of different components due to its versatile nature which does not require any major tooling or changes in the system. Third, (i) the availability of affordable implant materials such as metallic thin films/meshes/wires and oxides,^{3–5,15} carbon,^{1,5} i.e., carbon nanotubes (CNTs),^{15–17,19,20,22–24} and conducting polymers (CPs),^{5,6,10,18,21,25} (ii) the possibility of welding intricate¹ 3D joint geometries with high manufacturing rates and consistency,^{3,5} and (iii) the possibility of achieving superior joint qualities can be considered as the other reasons for the wide industrial exploitation of MW welding.⁵ The negligible disadvantages of the MW welding process includes the need for a consumable MW susceptible ancillary material¹² at the joint interface, which requires an additional stage in the process and may raise recycling issues, and bulk TPMs with polar

molecular groups used for the process, which might heat up rapidly and get thermally decomposed if the process parameters are not precisely controlled.

Throughout the last couple of decades a great deal of research effort has been spent for a unique class of materials called CPs. Recently, these materials have been facilely synthesized in different nanosized morphologies^{26–28} with the help of improvements in relevant science and technology. Within CPs family, polypyrrole (PPy) has been one of the most well-known and intensively studied members. PPy has many advantages such as simple and straightforward synthesis possibility at ambient conditions with low cost and high polymerization yield, long-term environmental stability, superior electrochemical properties, relatively high electrical conductivity, and tunable (acid/base) doping/dedoping characteristics, which is governed by the chain nitrogen in its structure.^{5,6,26}

As the MW absorbing active material for TPMs' welding process, CPs' use was first proposed 20 years after the revival of research interest in this field, which has increased exponentially since then.^{5,29} On the basis of the previous study results and the relevant information, CPs offer a promising potential for MW welding, which depends on their interactions with MW energy that can be altered through the systematic use of acidic dopants with electron-withdrawing amine (−NH), carboxyl (−COOH), carbonyl (−CO), and hydroxyl (−OH) groups.^{1,3,5,9,10} Depending on their doping levels, CPs would exhibit higher current carrying potential and dielectric loss,^{3,5,6,29} become more susceptible to MWs, and can absorb more energy, unlike transparent polymers or reflective metals.^{1,7,9,12,15,21} Another critical reason is related to CPs' morphology in nanosize, which is more suitable for the formation of substantial bonds and increased miscibility in the new welds at TPMs' interface through their highly active rough surface area.^{2,10} This can be given as the summary of the rationale behind the choice of nanosized PPy as the material of preference for the MW-based welding applications.

The well-established and previously used MW energy-based nanocarbonization³⁰ and in situ CNT growth technique^{27,31–33} called "PopTube approach" was simply modified and used in the current study to propose a simple, efficient, affordable, and easily mass-production adaptable welding process. The method can be simply summarized as short-term MW heating of a specific composite, made up of PPy nanogranule (NG) coated carbon and catalyst source precursor (ferrocene) fine particles, at different size polypropylene (PP) dog bone specimens' interface for simultaneous carbonization and in situ CNT growth. To the best of our knowledge, for the first time, the above-mentioned advantages of MW welding process and the reinforcing features of in situ grown CNTs at the weld area were efficiently combined to reach superior mechanical properties in the newly formed welds. Such welds were

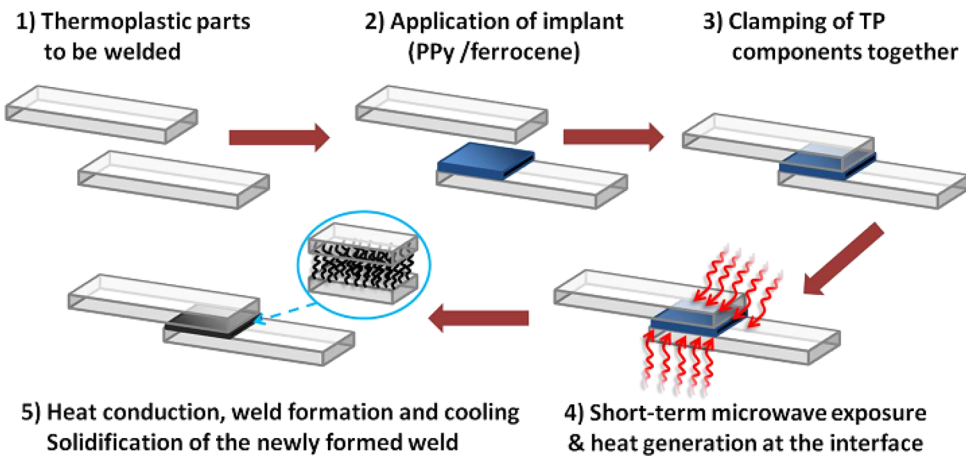


Figure 1. Schematic representation of MW welding of TPMs through nano-CP-based implant composite.



Figure 2. Representation of PP dog bone specimens and their area locations used for mechanical property calculations as given in [Table 1](#) (left), digital images of both the experimental setup (middle), and the welded small dog bone sample fixed between clamps (right).

Table 1. Total Process Times for PP Dog Bone Specimens Based on Their Dimensions and PPy/Ferrocene Amount at Their Interface

specimen	nonwelded area (mm ²)	PPy/ferrocene amount (mg)	total process time (s)	W × L × T (mm)	avg. welded area (mm ²)
big dog bone	480	25	30–35	18 × 31–33 × 3	576
straight dog bone	480	15	20–25	13 × 18–21 × 3	234
small dog bone	75	10	10–15	9 × 20 × 2	180

mechanically tested by means of lap shear strength, and the morphological features with detailed elemental analysis of the as-grown CNTs at the weld interface were also conducted via electron microscopy to prove the success of this novel methodology.

MATERIALS AND METHODS

Materials. Pyrrole, ferrocene, and ammonium peroxydisulfate ($(\text{NH}_4)_2\text{S}_2\text{O}_8$, APS) were all purchased from Alfa Aesar and used as-received. Another reagent, hydrochloric acid (HCl), was received at analytical grade from J.T. Baker and used without further purification. Differently sized PP dog bone specimens were obtained by processing PP chips (Exxon Mobil) in a Battenfeld EM 50/300 injection molding machine.

One-Step Synthesis of PPy/Ferrocene Composite (Scheme 1). In a typical experiment, 1 g of fine ferrocene particles were added into 50 mL of 1 M aqueous (aq.) HCl under vigorous magnetic stirring. After 5 min of stirring at ambient conditions, 1 mL of pyrrole monomer was added into this medium. Two reagents were stirred constantly for another 5 min, to achieve more homogeneous dispersion. Lastly, 1.15 g of APS was added into the reaction vessel, with rapid darkening in reaction medium color, to initiate the polymerization reaction that lasted for 4 h. At the end of the polymerization/coating reaction, the dark PPy/ferrocene precipitate

was suction-filtered while getting washed with copious amounts of 1 M aq. HCl (3 × 100 mL) and acetone (3 × 100 mL), respectively. The as-obtained sample was collected from the filter paper and allowed to dry overnight at ambient conditions. Finally, the sample was gently crushed into small chunks, placed in a plastic cup, and processed in a speed mixer at 3500 rpm to gain its fine powder form.

MW Welding of PP Dog Bone Pieces via in Situ Nano-carbonization and CNT Growth (Figure 1). From the as-prepared PPy/ferrocene composite, certain amounts were weighed and placed at the interfaces of big, small, and straight PP dog bone specimens, respectively (Figure 2). The fine powder form composite was homogeneously spread on the surface with a steel spatula. Next, PP dog bone couples on a glass slide were carefully placed into the MW chamber (Panasonic Inverter) with a watch glass or beaker load on top of them to apply the required pressure during short-term MW heating process. Depending on their dimensions and the weight fraction of PPy/ferrocene composite at their interface (Table 1), PP substrates were irradiated with 1250 W MW energy for specified durations. Eventually, the MW power was turned off and the as-welded PP sample was taken out from the MW chamber for the final cooling and solidification step. During this step, external light pressure could be manually applied onto the new weld, to ensure (i) more homogeneous heat distribution within the welding area, (ii) the minimization of possible shape changes, and (iii) the prevention of excessive molten material squeeze out, for better results.

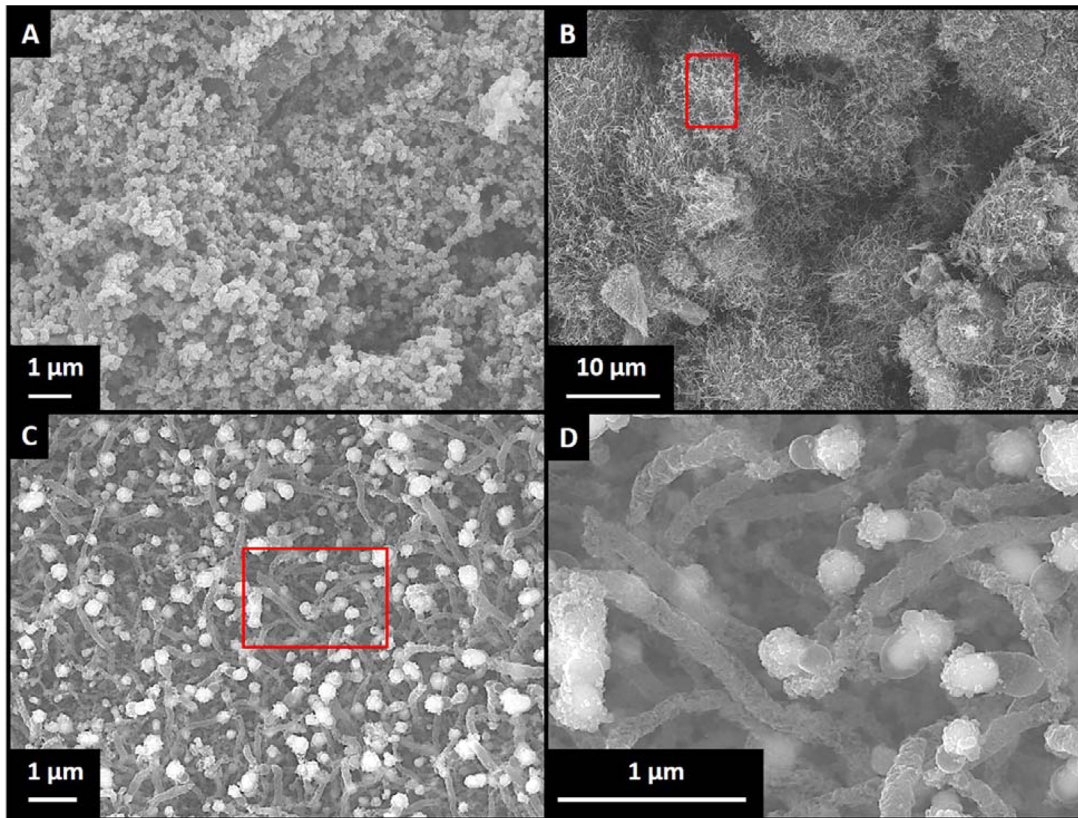


Figure 3. SEM images: (A) PPy NG coating on the surface of fine ferrocene particles; (B) as-grown CNTs on the surface of PPy NG coating after short-term MW irradiation; (C) and (D) detailed, zoomed-in views of the micrometer-long, tip-grown CNTs with nanogranular iron tips at the red rectangular areas marked in (B) and (C), respectively.

Characterization of the As-Obtained Welds. In-depth morphological and elemental analyses of different nanocarbons formed in the welding area were done by using a JEOL JSM-7000F scanning electron microscope (SEM) equipped with an energy dispersive X-ray (EDX) detector. Lap shear and tensile strength measurements of the nonwelded/welded PP samples were conducted at standard laboratory conditions by using the Instron 5565 universal testing machine equipped with Bluehill software. Here, there was only one method generated from the software and used for both types of samples to determine their mechanical properties. Before starting the tests, the required test parameter, i.e., length of the weld interface, was entered individually in the program since the width of each welded dog bone sample was selected as the constant value. Although the thickness has a direct influence on MWs' ability to penetrate into the weld interface and therefore the welding time and final quality, its value was neglected for the mechanical testing of as-welded samples. Next, the sample was placed vertically between the clamps and it was fixed by pneumatic pedals controlling these clamps, as shown in Figure 2. Initially, the samples were applied a preload of 1 N to get rid of any residual stress left in them. After that, clamps started extending the samples at a constant crosshead speed of 2 mm/min until they were broken. As soon as the sample was broken, the clamps automatically returned to their original positions and the sample was taken off them to start testing a new sample.

RESULTS AND DISCUSSION

Figures 3 and 4 provide detailed information about the morphological features of PPy NG and the as-grown CNTs in the welding area. PPy NG clusters can be clearly observed as a coating on fine ferrocene particles surface in Figure 3A. The majority of the NG clusters have the average outer diameter size in the range of 250–430 nm.³² This is also consistent both with the inherent morphology of PPy obtained from HCl and

with the data from previous literature.²⁷ After short-term irradiation by MWs, the surface of PPy NG coating was decorated with the as-grown multiwalled CNTs (Figure 3B). The homogeneity and coverage density of the in situ grown CNTs were observed to be very high since in this case the precursor ferrocene particles were directly covered by the heat source, i.e., conducting PPy NGs, instead of getting mixed with them as in previous studies.^{27,31–33} The zoomed-in view of the CNTs marked in the rectangular area of the same figure can be seen in Figure 3C. This result provides solid proof for the presence of micrometer-long, as-grown CNTs decorating the PPy NG surface area. A more detailed view of such CNTs could be observed in Figure 3D. This figure clearly exhibited the morphological features of micrometer-long and highly porous CNTs with ~250 nm average diameter iron oxide NG clusters at their tips. These results were coinciding with the ones from similar studies in the literature, and were once more confirming the tip-growth mechanism for the as-obtained CNTs.^{27,31–33}

From a slightly different perspective, it is possible to observe how both the as-grown CNTs and the welding area look like after the mechanical properties of the welded dog bone pieces were tested, in Figure 4. Broken with the applied shear stress, the CNTs grown through PPy NG coating can be clearly observed in Figure 4A. It is also possible to observe from the zoomed-in view of the marked rectangular area in Figure 4B that the carbonized PPy NG coating covered the as-grown CNTs like sheath. Moreover, bamboo shoot or earthwormlike, micrometer-long broken CNTs grown through the carbonized PPy NG coating can be seen from Figure 4C. It is also obvious

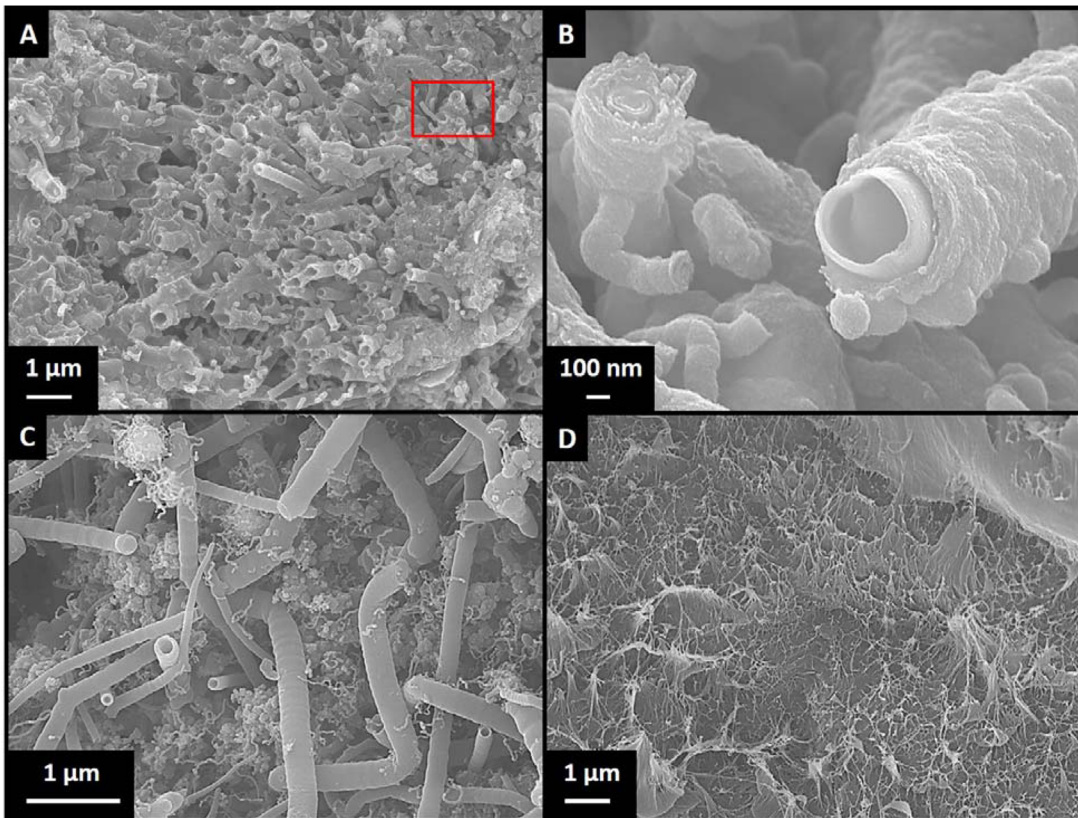


Figure 4. SEM images: (A) as-grown CNTs within the carbonized PPy NG coating; (B) zoomed-in view of the red rectangular area marked in (A) showing CNTs covered by carbonized PPy NG coating; (C) bamboo shoot or earthwormlike CNTs grown through the carbonized PPy NG coating with secondary growth on their surface; (D) networks of the as-grown CNTs penetrating into the sheared PP dog bone surface.

to see the secondary growth on these tubes, which is a common phenomenon that occurs when ferrocene, as both the carbon and catalyst source, is abundant.^{27,31} Last but not least, networks of the as-grown CNTs protruding from the sheared welding interface could be clearly observed in Figure 4D. This was crucial evidence for the success of this study that proved how the as-grown CNTs penetrate into the TPM specimens, as reinforcing agents, during short-term MW welding process.^{16,17,20,22–24}

After the presence of the in situ grown CNTs in the welding area was confirmed through electron microscopy, their elemental analysis results were also acquired through EDX as supplementary data. There were two spectra selected to detect the elements included in both the stems and the tips of the as-grown CNTs, as shown in Figure 5A. On the basis of the summarized results in Table 2, (i) the tips of CNTs were comprised of iron oxide NGs as mentioned earlier and (ii) the stems of CNTs were majorly composed of carbon and iron, as an expected result upon the use of ferrocene as a precursor material for CNT growth. In addition, the presence of gold (Au) element in the analysis results was due to the plasma coating applied on the as-prepared samples before SEM imaging/EDX analysis.

Morphological and elemental analysis results of the nanostructured carbon composite sample in the welding area of the PP dog bone specimens provided very useful information. However, without mechanical property analysis results the study would not be complete. Therefore, with use of the Instron 5565 universal testing machine equipped with Bluehill software, the tensile strengths of nonwelded PP dog bone

specimens and the lap shear strengths (LSS, τ) of welded PP dog bone couples were tested, as explained earlier. The stress-strain ($\sigma-\epsilon$) graphics shown in Figure 6 A–C represent the behaviors of nonwelded big, straight, and small PP dog bone samples, respectively. The maximum stress (σ_{\max}) of each type of nonwelded sample was taken into account for comparisons with the welded samples. The results are summarized in Table 3. As for the welded samples' LSS results, it was calculated with the formula

$$\tau = \frac{\sigma_{\max}}{W \times L}$$

where W and L represent the dimensions of the weld area given in Table 1. On the basis of the $\sigma-\epsilon$ graphics shown in Figure 6 D–F, σ_{\max} values of each type of welded sample are given in Table 3. These results clearly prove the success of this novel welding technique, where the majority of σ_{\max} values of welded samples were retained compared to their nonwelded versions.

Although there was no difference in their preparation steps, there are some insignificant variations in the welded dog bone specimens' LSS results. Such variations are majorly caused by the geometrical differences among those specimens, which could make a big difference in their final weld properties. Thus, for the specimens with larger surface area, (i) there would be more PPy/ferrocene at their interface and so (ii) they can absorb the MW energy more efficiently and (iii) they could form more robust welds compared to the ones with smaller surface area. A similar debate can be made on the reinforcing effect of the as-grown CNTs at the welding area, which was less than expected for the smaller area samples. Several possible

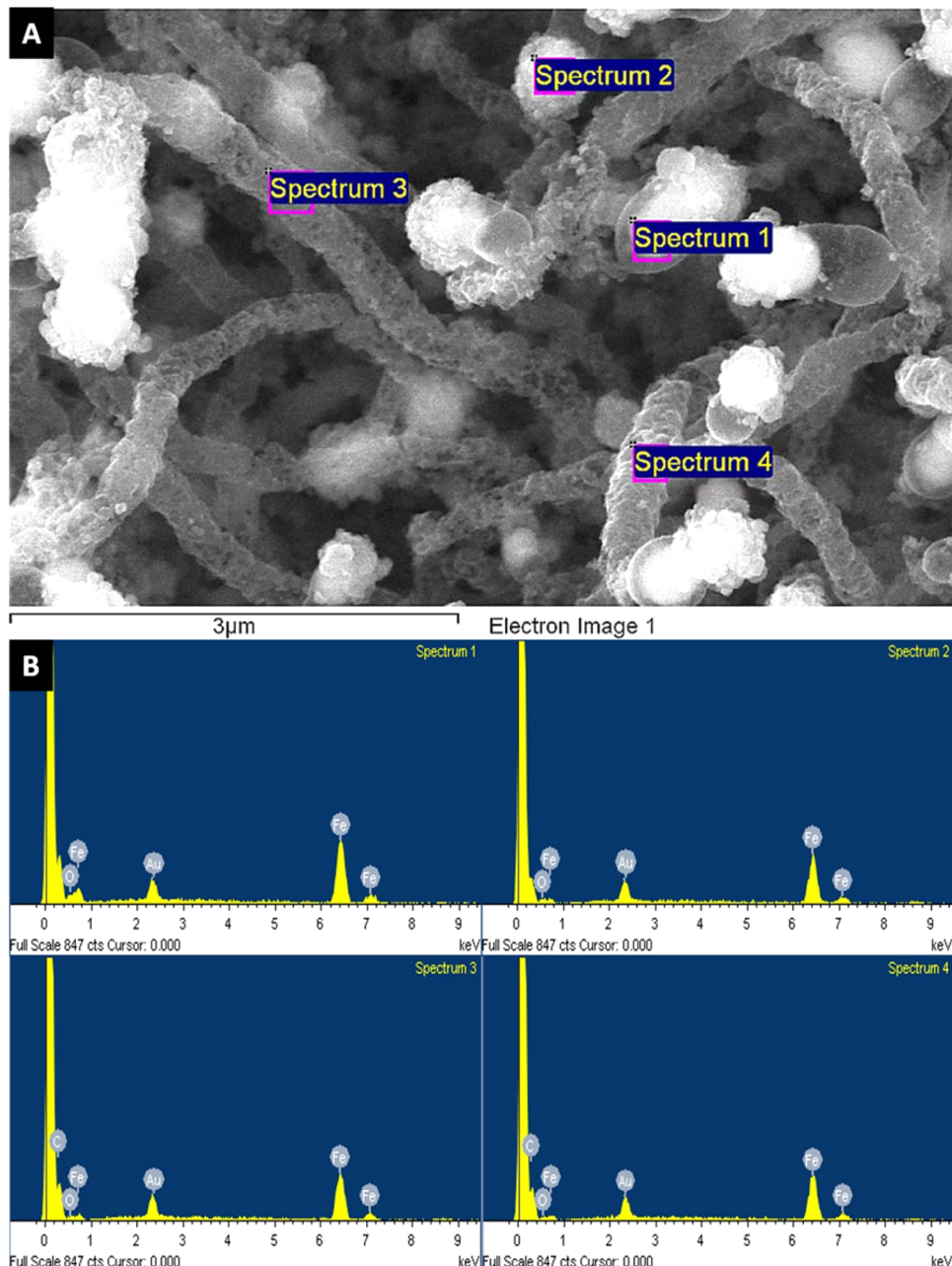


Figure 5. (A) SEM image used for the elemental analysis of the as-grown CNTs; (B) EDX analysis results for each selected spectrum on the SEM image.

Table 2. Summary of the Percentage of Elements from EDX Analysis Results Shown in Figure 5B

spectrum	C	O	Fe	total
1		27.9	72.1	100
2		26.2	73.8	100
3	88.7		11.3	100
4	87.6		12.4	100

reasons of this phenomenon can be listed as (i) the randomness in CNT growth pattern, which was not in the ideal form of a perfectly aligned vertical forest, because of the random placement of ferrocene particles at the weld interface, (ii) the size range of ferrocene particles, which were quite large and caused a decrease in the number of penetrations that could have been made by the as-grown CNTs (larger distance

between PP bulks, less chance for the formation of anchoring points by CNTs), and (iii) the unexpected heat deformations in the weld structure caused by CNT growth. Since the active PPy/ferrocene layer was applied in powder form, upon the decomposition of ferrocene for CNT growth, the as-generated vapor could be trapped in the molten PP and lead to the formation of unexpected bubbles as the weak spots in the structure. All these phenomena could negatively affect the LSS results and hinder the expected reinforcement effect provided by CNT growth. After all, it should be noted that the as-obtained welds were not lacking CNT reinforcement effect since the LSS results from the welded big dog bone specimens showed 95–98% σ_{max} retention in their results, compared to their nonwelded versions.

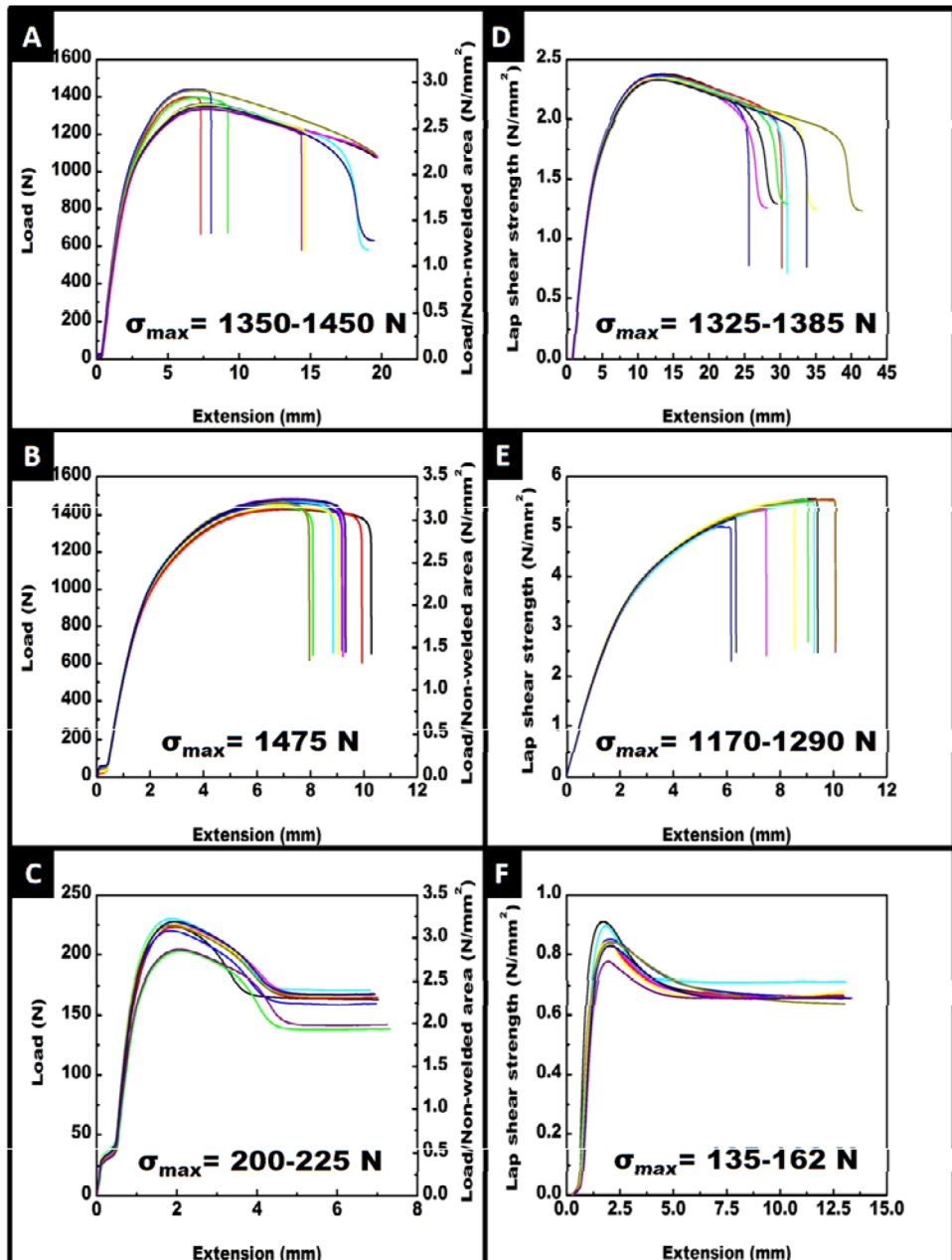


Figure 6. σ - ε graphics of (A, B, C) nonwelded and (D, E, F) welded big, straight, and small dog bone samples, respectively.

Table 3. Summary of the Tensile and LS Strength Results Shown in Figure 6

σ_{\max} (N)	big dog bones	straight dog bones	small dog bones
nonwelded	1350–1450	1475	200–225
welded	1325–1385	1170–1290	135–162
σ_{\max} retention (%)	95.5–98	79.3–87.45	62.5–72

The following plausible working mechanism is meant to provide a better understanding for this novel methodology. The MW energy-based welding process can be simply explained with the electromagnetic interactions between incident MWs and PPy NG coating on the ferrocene precursor. Here, the essential material property that governs such interactions is the dielectric property. In the current process, separate PP dog bone substrates containing PPy/ferrocene composite at their interface were kept together under a clamp to ensure better

contact with each other. Next, the couple's interface was irradiated by short-term MW energy which was delivered via a multimode magnetron operating at 2.45 GHz. Differently from other conventional heating methods, in a MW oven, the material's heating process occurs selectively in a volumetric manner. Therefore, only the MW susceptible portion of the material, in this case PPy/ferrocene containing interface area, would gain the heat. The HCl-doped PPy NG coating on fine ferrocene particles' surface would absorb the MW energy, start sparking and arcing vigorously with an instant temperature rise above 1000 °C, and eventually get carbonized.^{27,31,32} At this point, the organometallic precursor particles underneath were rapidly decomposed to iron and cyclopentadienyl groups that would serve as the catalyst and carbon source for in situ CNT growth at the welding interface.^{27,31–33} Although the formation mechanism of such CNTs are not very clear, we believe that the iron from the decomposed ferrocene had served as the active

catalyst and the pyrolyzed carbons from the cyclopentadienyl ligands had been realigned to form CNTs while carrying the active iron, in NP cluster form, up to their tips.^{27,32,33} The above-mentioned SEM and EDX characterization results are strongly supporting the proposed mechanism as well. Meanwhile, the dissipated energy was effectively conveyed through both the carbonized PPy and the as-formed CNTs into the adjacent PP dog bone surface to raise its temperature to its melting point.^{6,17} Next, PP molecules at close proximity started to flow and eventually formed a new weld upon either formation of covalent bonds or cross-links with carbonized PPy NGs or diffusion in a network form among the as-grown CNTs.^{10,11,16} Finally, the MW power was turned off and all the above-mentioned components came into intimate contact. After the welded dog bone couple was taken out from the MW chamber, external pressure was gently applied on the welding area, to increase the integrity of the new weld,²¹ during cooling and solidification steps.¹⁸

Lastly, it is essential to understand the synergistic nature²⁵ of this novel welding technique, to determine and evaluate its success. Here, the final weld quality and the fate of MW welded TPMs*** were affected by many parameters, the most important of which are the electrical and morphological properties of the MW susceptible (CP) material used. In this case, since the electrical conductivity of PPy could be easily tuned via HCl doping and since it had NG morphology, PPy would effectively absorb the MW energy and convert it into heat that was required for its carbonization and in situ CNT growth at the welding interface, without causing any thermal deformation on the TPM substrates.^{4,10} The length of the MW heating (process) time is another crucial parameter of this novel process. It is mainly dependent on both the above-mentioned properties of the MW susceptible material and the TPM used. With respect to MW welding technique's universal nature, it is easy to optimize the heating time by simply matching the ideal material couple that would be used for this process.⁶ The external pressure applied during and after the welding process is another important parameter, whose influence on the final weld quality was indicated and proved in many previous studies.^{2,6,10,25} Additionally, the effect of CP's weight fraction on the final mechanical properties of the new weld was also investigated.^{6,15,18} It was proven in many studies that through the optimization of weight fraction the final weld strength could be facilely adjusted and its value could approach that of the pristine TPM's used for the study.¹² This parameter is also crucial to achieve both the desired heating pattern and correct location of the new weld.^{2,21}

CONCLUSION

For the first time, within this study, PPy NGs were used as an active MW absorbing coating on carbon and catalyst source precursor (ferrocene) particles' surface for in situ CNT growth via short-term MW irradiation to weld TPMs in a clean, reliable, and facile manner without causing any thermal deformation in the bulk PP dog bone substrates. The electron microscopy, elemental analysis, and mechanical property characterization results of the as-obtained welds were also clearly indicating the success of this novel methodology. Along with the data from the previous literature, the superiority of the MW welding technique over other conventional methods was also clearly stated through detailed expression of its tangible advantages such as selective and volumetric heating of the MW absorbing weld interface, efficient processing opportunity of

complex shapes, easily controllable process parameters and extent, and final products with enhanced physical/mechanical properties. Furthermore, considerable benefits of using nano-CPs for joining and repair of TPM composites via short-term MW heating was also elucidated. Although it is still in a development stage and further research needs to be conducted to acquire a full understanding of its underlying principles, we believe that the MW energy-based TPM welding technique offers a vast potential and will gain great commercial significance through effective and efficient mass production of next-generation TPM composites at industrial scale.

AUTHOR INFORMATION

Corresponding Author

*Tel.: 334-844-5439. Fax: 334-844-4068. E-mail: xzz0004@auburn.edu.

Notes

The authors declare no competing financial interest.

ACKNOWLEDGMENTS

We gratefully acknowledge financial support from NASA award NNX14AF49A.

REFERENCES

- (1) Aravindan, S.; Krishnamurthy, R. Joining of Ceramic Composites by Microwave Heating. *Mater. Lett.* **1999**, *38*, 245–249.
- (2) Olofinjana, A.; Yarlagadda, P. K. D. V.; Oloyede, A. Microwave Processing of Adhesive Joints Using a Temperature Controlled Feedback System. *Int. J. Mach. Tools Manuf.* **2001**, *41*, 209–225.
- (3) Varadan, V. K.; Varadan, V. V. Microwave Joining and Repair of Composite-Materials. *Polym. Eng. Sci.* **1991**, *31*, 470–486.
- (4) Lause, H. J.; Parks, K. L.; Tanis, L. D.; Leon, D. D. Method of Welding Thermoplastic Substrates with Microwave Frequencies. U.S. Patent 5338611, 1994.
- (5) Wise, R. J.; Froment, I. D. Microwave Welding of Thermoplastics. *J. Mater. Sci.* **2001**, *36*, 5935–5954.
- (6) Wu, C. Y.; Benatar, A. Microwave Welding of High Density Polyethylene Using Intrinsically Conductive Polyaniline. *Polym. Eng. Sci.* **1997**, *37*, 738–743.
- (7) Clark, D. E.; Folz, D. C.; West, J. K. Processing Materials with Microwave Energy. *Mater. Sci. Eng., A* **2000**, *287*, 153–158.
- (8) Thostenson, E. T.; Chou, T. W. Microwave Processing: Fundamentals and Applications. *Composites, Part A* **1999**, *30*, 1055–1071.
- (9) Siores, E.; Dorego, D. Microwave Applications in Materials Joining. *J. Mater. Process. Technol.* **1995**, *48*, 619–625.
- (10) Kathirgamanathan, P. Microwave Welding of Thermoplastics Using Inherently Conducting Polymers. *Polymer* **1993**, *34*, 3105–3106.
- (11) Huang, J. X.; Kaner, R. B. Flash Welding of Conducting Polymer Nanofibres. *Nat. Mater.* **2004**, *3*, 783–786.
- (12) Potente, H.; Karger, O.; Fiebler, G. Laser and Microwave Welding - The Applicability of New Process Principles. *Macromol. Mater. Eng.* **2002**, *287*, 734–744.
- (13) Mapleton, P. Plastics Welding: The Choices Widen. *Plast. Eng.* **2008**, *64*, 10–16.
- (14) Yarlagadda, P. K. D. V.; Chai, T. C. An Investigation into Welding of Engineering Thermoplastics Using Focused Microwave Energy. *J. Mater. Process. Technol.* **1998**, *74*, 199–212.
- (15) Harper, J. F.; Price, D. M.; Zhang, J. Microwave Forming and Welding of Polymers. *10th International Conference on Microwave and High Frequency Heating* **2005**, 298–301.
- (16) Wu, T. F.; Pan, Y. Z.; Liu, E. J.; Li, L. Carbon Nanotube/Polypropylene Composite Particles for Microwave Welding. *J. Appl. Polym. Sci.* **2012**, *126*, E283–E289.

- (17) Wang, C. Y.; Chen, T. G.; Chang, S. C.; Cheng, S. Y.; Chin, T. S. Strong Carbon-Nanotube-Polymer Bonding by Microwave Irradiation. *Adv. Funct. Mater.* **2007**, *17*, 1979–1983.
- (18) Wu, C. Y.; Staicovici, S.; Benatar, A. Microwave Welding of HDPE Using Impedance Matching System. *J. Reinforced Plast. Compos.* **1999**, *18*, 27–34.
- (19) Xie, R.; Wang, J. P.; Yang, Y.; Jiang, K. L.; Li, Q. Q.; Fan, S. S. Aligned Carbon Nanotube Coating on Polyethylene Surface Formed by Microwave Radiation. *Compos. Sci. Technol.* **2011**, *72*, 85–90.
- (20) Wang, C. Y.; Chen, T. H.; Chang, S. C.; Chin, T. S.; Cheng, S. Y. Flexible Field Emitter Made of Carbon Nanotubes Microwave Welded onto Polymer Substrates. *Appl. Phys. Lett.* **2007**, *90*, 103111–103113.
- (21) Yussuf, A. A.; Sbarski, I.; Hayes, J. P.; Solomon, M.; Tran, N. Microwave Welding of Polymeric-Microfluidic Devices. *J. Micromech. Microeng.* **2005**, *15*, 1692–1699.
- (22) Zhang, M.; Fang, S. L.; Zakhidov, A. A.; Lee, S. B.; Aliev, A. E.; Williams, C. D.; Atkinson, K. R.; Baughman, R. H. Strong, Transparent, Multifunctional, Carbon Nanotube Sheets. *Science* **2005**, *309*, 1215–1219.
- (23) Han, J. T.; Kim, D.; Kim, J. S.; Seol, S. K.; Jeong, S. Y.; Jeong, H. J.; Chang, W. S.; Lee, G.-W.; Jung, S. Self-Passivation of Transparent Single-Walled Carbon Nanotube Films on Plastic Substrates by Microwave-Induced Rapid Nanowelding. *Appl. Phys. Lett.* **2012**, *100*, 163120–163124.
- (24) Shim, H. C.; Kwak, Y. K.; Han, C. S.; Kim, S. Enhancement of Adhesion Between Carbon Nanotubes and Polymer Substrates Using Microwave Irradiation. *Scr. Mater.* **2009**, *61*, 32–35.
- (25) Staicovici, S.; Wu, C. Y.; Benatar, A. Welding and Disassembly of Microwave Welded HDPE Bars. *J. Reinforced Plast. Compos.* **1999**, *18*, 35–43.
- (26) Liu, Z.; Liu, Y.; Poyraz, S.; Zhang, X. Y. Green-Nano Approach to Nanostructured Polypyrrole. *Chem. Commun.* **2011**, *47*, 4421–4423.
- (27) Liu, Z.; Wang, J. L.; Kushvaha, V.; Poyraz, S.; Tippur, H.; Park, S.; Kim, M.; Liu, Y.; Bar, J.; Chen, H.; Zhang, X. Y. Poptube Approach for Ultrafast Carbon Nanotube Growth. *Chem. Commun.* **2011**, *47*, 9912–9914.
- (28) Liu, Z.; Zhang, X. Y.; Poyraz, S.; Surwade, S. P.; Manohar, S. K. Oxidative Template for Conducting Polymer Nanoclips. *J. Am. Chem. Soc.* **2010**, *132*, 13158–13159.
- (29) Epstein, A. J.; Macdiarmid, A. G. Polyanilines - from Solitons to Polymer-Metal, from Chemical Curiosity to Technology. *Synth. Met.* **1995**, *69*, 179–182.
- (30) Zhang, X. Y.; Manohar, S. K. Microwave Synthesis of Nanocarbons from Conducting Polymers. *Chem. Commun.* **2006**, *23*, 2477–2479.
- (31) Liu, Z.; Zhang, L.; Poyraz, S.; Smith, J.; Kushvaha, V.; Tippur, H.; Zhang, X. Y. An Ultrafast Microwave Approach towards Multicomponent and Multi-Dimensional Nanomaterials. *RSC Adv.* **2014**, *4*, 9308–9313.
- (32) Poyraz, S.; Liu, Z.; Liu, Y.; Zhang, X. Y. Devilcanization of Scrap Ground Tire Rubber and Successive Carbon Nanotube Growth by Microwave Irradiation. *Curr. Org. Chem.* **2013**, *17*, 2243–2248.
- (33) Xie, H.; Poyraz, S.; Thu, M.; Liu, Y.; Snyder, E. Y.; Smith, J. W.; Zhang, X. Y. Microwave-Assisted Fabrication of Carbon Nanotubes Decorated Polymeric Nano-Medical Platforms for Simultaneous Drug Delivery and Magnetic Resonance Imaging. *RSC Adv.* **2014**, *4*, 5649–5652.